Electronic structure and magnetic properties of the spin-1/2 Heisenberg system $CuSe_2O_5$

View the article online for updates and enhancements.

Electronic structure and magnetic properties of the spin-1/2 Heisenberg system $CuSe_2O_5$

O Janson[1,4]**, W Schnelle**[1]**, M Schmidt**[1]**, Yu Prots**[1]**,
S-L Drechsler**[2]**, S K Filatov**[3] **and H Rosner**[1,4]

[1] Max-Planck-Institut für Chemische Physik fester Stoffe,
Nöthnitzer Straße 40, 01187 Dresden, Germany
[2] Leibniz-Institut für Festkörper- und Werkstoffforschung Dresden,
PO Box 270116, 01171 Dresden, Germany
[3] Department of Crystallography, St Petersburg State University,
Universitetskaya Naberezhnaya 7/9, St Petersburg, 199034, Russia
E-mail: rosner@cpfs.mpg.de and janson@cpfs.mpg.de

Abstract. A microscopic magnetic model for the spin-1/2 Heisenberg chain compound $CuSe_2O_5$ is developed based on the results of a joint experimental and theoretical study. Magnetic susceptibility and specific heat data give evidence for quasi-one-dimensional (1D) magnetism with leading antiferromagnetic (AFM) couplings and an AFM ordering temperature of 17 K. For microscopic insight, full-potential density functional theory (DFT) calculations within the local density approximation (LDA) were performed. Using the resulting band structure, a consistent set of transfer integrals for an effective one-band tight-binding model was obtained. Electronic correlations were treated on a mean-field level starting from LDA (LSDA $+ U$ method) and on a model level (Hubbard model). With excellent agreement between experiment and theory, we find that only two couplings in $CuSe_2O_5$ are relevant: the nearest-neighbour intra-chain interaction of 165 K and a non-frustrated inter-chain (IC) coupling of 20 K. From a comparison with structurally related systems ($Sr_2Cu(PO_4)_2$, Bi_2CuO_4), general implications for a magnetic ordering in presence of IC frustration are made.

[4] Authors to whom any correspondence should be addressed.

Contents

1. Introduction

Low-dimensional spin-1/2 systems attract much interest due to a variety of ground states (GSs) found in these systems which originates from an interplay between different exchange interactions and strong quantum fluctuations. There are, for instance, the spin-Peierls GS in $CuGeO_3$ [1], the helical GS in $LiCuVO_4$ [2], and the quantum critical behaviour in Li_2ZrCuO_4 [3, 4] etc. Besides, many of these materials (mostly cuprates, vanadates and titanates) appeared to be realizations of theoretically long-studied models to a good approximation. One of the most prominent models is the spin-1/2 nearest-neighbour (NN) chain described by the Heisenberg Hamiltonian, for which the exact solution has been derived by Bethe [5]. The first compounds proposed to be good material realizations of this model were Sr_2CuO_3 and Ca_2CuO_3 [6, 7]. Recently, $Sr_2Cu(PO_4)_2$ and $Ba_2Cu(PO_4)_2$ were suggested as even better realizations [8]–[12], followed by a study of $K_2CuP_2O_7$ [13] that qualified this compound to be the best realization of the spin-1/2 NN Heisenberg chain to date. As a natural consequence of its simplicity, this model poorly describes one-dimensional (1D) and quasi-1D systems where additional interactions, like longer range couplings or anisotropies, are present. Thus, extensions of this model are required to allow an accurate description of real materials.

The simplest extension of the model is the inclusion of a next-nearest-neighbour (NNN) coupling J_2 leading to the so-called zigzag chain model. In case of an antiferromagnetic (AFM) J_2 both NN and NNN couplings cannot be simultaneously satisfied; in other words, the system is magnetically frustrated. Here, the intra-chain frustration enriches the phase diagram with the spiral GS, the gapped AFM GS and a quantum critical point at $J_2/J_1 = -0.25$ [14]–[17]. The evaluation of the two parameters in the zigzag chain model allows one to estimate quantities which can be directly measured or derived from experiments, namely spin–spin correlation functions, thermodynamic properties and the response in high magnetic fields. Nevertheless, this model fails to describe phenomena like long-range magnetic ordering, since 1D or 2D systems do not order collinearly at finite temperatures according to the Mermin–Wagner theorem [18]. Thus, to account for magnetic ordering, the inter-chain (IC) coupling has to be included in the model. This problem has been addressed in a series of theoretical works [19]–[26], but the simplifications that had to be made to keep the models solvable (at least approximately) impede an accurate description of complex situations. The spin-1/2 Heisenberg chain system

$Sr_2Cu(PO_4)_2$ is the most prominent example for a huge discrepancy (two orders of magnitude) between the theoretical (adopting a simple NN IC coupling) and the experimentally observed ordering temperature. The origin of this discrepancy is hidden in the effects of magnetic frustration and anisotropy, and the disentanglement of the effects is difficult. Thus, a reliable theoretical description of this phenomenon is still lacking.

A natural way towards a deeper understanding is the search for real material realizations of 'easy' models. For such systems, the experimental data can be supplemented by reliable microscopic models. In this way, joint experimental and theoretical studies can challenge and improve the existing theoretical approaches.

Cu^{2+} phosphates are to date the best realizations of the NN spin-1/2 Heisenberg chain model [8, 10, 13] and have a great potential for the discovery of further low-dimensional systems. Unfortunately, the experimental information about these materials is rather limited since they are up to now available as powders only, although several attempts have been made to grow single crystals required for advanced experimental studies.

In this paper, the structurally closely related compound, $CuSe_2O_5$, is investigated. Since selenites are often susceptible to chemical transport, the advantage of this material is the potential to grow large single crystals of high quality. Previous studies on a powder sample [27] may hint at a 1D character of its magnetic properties, but the low-temperature data are strongly affected by impurities (figure 3 in [27]). Therefore, to probe the 1D nature of the system, a new detailed study on high quality samples with lower defect concentration is desirable.

Though the chain-like arrangement of CuO_4 squares in $CuSe_2O_5$ is topologically similar to that in Cu^{2+} phosphates, the geometry of magnetic coupling paths between the structural chains is essentially different. Thus, the role of magnetic frustration, which is ruled by the IC coupling, can be evaluated in a comparative study.

The paper is organized as follows. In section 2, we describe the synthesis, sample characterization and experimental as well as theoretical methods used in this work. In section 3, we discuss the crystal structure of $CuSe_2O_5$ in comparison to related systems. Section 4 reports the results of our measurements and theoretical calculations and proposes an appropriate microscopic model. A brief summary and an outlook are given in section 5.

2. Method and sample characterization

Single crystals of $CuSe_2O_5$ were grown by chemical vapour transport using $TeCl_4$ as a transport agent. Using a micro-crystalline powder of $CuSe_2O_5$ (obtained from a mixture of CuO and SeO_2 at 723 K) as a source, the transport experiments were carried out in an endothermic reaction of T_2 (source) 653 K to T_1 (sink) 553 K.

The obtained crystals have a green colour and form strongly elongated (along [001]) plates, which macroscopically look like needles. The typical length of a needle is 5–10 mm and the width does not exceed 1 mm and for most crystallites it is considerably smaller. The slight disorientation of plates forming a needle necessitates a precise x-ray diffraction measurement on single crystals. Thus, the samples were characterized by x-ray powder diffraction and energy-dispersive x-ray spectroscopy (EDXS) experiments. The lattice parameters of the synthesized crystals are similar to those reported for $CuSe_2O_5$ (table 1). The results of the EDXS analysis (Cu32.78 ± 0.31, Se67.14 ± 0.23) for 13 points (2 crystals) yield Cu : Se ≈ 0.488 ± 0.006, close to the ideal ratio of 0.5. Thus, the obtained single crystals represent an almost pure $CuSe_2O_5$ phase.

Table 1. Comparison of measured lattice parameters a, b, c, the monoclinic angle β and the unit cell volume V of $CuSe_2O_5$ with previously published data.

Parameter	Ref. [38]	Ref. [37]	This work
a (Å)	12.3869	12.254	12.272
b (Å)	4.8699	4.858	4.856
c (Å)	7.9917	7.960	7.975
β (°)	109.53	110.70	110.91
V (Å^3)	447.13	443.27	443.95

Magnetization was measured in a SQUID magnetometer (1.8–350 K) in magnetic fields up to 1 T. Heat capacity (1.8–100 K) was determined by a relaxation method up to $\mu_0 H = 9$ T.

Density functional theory (DFT) calculations were carried out using the full potential local orbital code (FPLO) version 7.00-27 [28] for the experimental structural parameters [38]. The standard basis set and the Perdew–Wang parameterization of the exchange-correlation potential were used [29]. Strong on-site Coulomb interaction in the Cu 3d orbitals, insufficiently described in the LDA, was taken into account independently (i) by mapping the local density approximation (LDA) antibonding Cu–O dpσ bands onto a tight-binding (TB) model ($\hat{H} = \sum_i \epsilon_i + \sum_{\langle ij \rangle \sigma} t_{ij} (c_{i,\sigma}^\dagger c_{j,\sigma} + \text{H.c.})$) and subsequently via a Hubbard model ($\hat{H} = \sum_i \epsilon_i + \sum_{\langle ij \rangle \sigma} t_{ij} (\hat{c}_{i,\sigma} \hat{c}_{j,\sigma}^\dagger + \text{H.c.}) + U_{\text{eff}} \sum_i \hat{n}_{i,\uparrow} \hat{n}_{i,\downarrow}$) onto a Heisenberg model ($\hat{H} = \sum_{\langle ij \rangle} J_{ij} \hat{\vec{S}}_i \hat{\vec{S}}_j$) (the procedure is well justified for spin excitations in the strongly correlated limit ($U_{\text{eff}} \gg t_{ij}$) at half-filling ($\langle n_i \rangle = 1$)) and (ii) using the LSDA + U method [30] ($U_d = 6.5$ eV, $J_d = 1$ eV). For the LDA calculations, we used a k-mesh of 1296 k-points (355 points in the irreducible wedge); for LSDA + U calculations of supercells irreducible k-meshes of 226, 242, 147 and 126 k-points were used. All k-meshes are well converged.

Quantum Monte Carlo (QMC) simulations were performed on $N = 1200$ sites clusters of $S = 1/2$ spins (30 coupled chains of 40 sites each) using the ALPS software package [31].

3. Crystal structure and empirical magnetic models

Crystal structures of cuprates are often subdivided into four large groups according to their dimensionality, which reflects how their elementary building blocks—CuO_4 plaquettes (planar or distorted)—are connected: they can be isolated (0D) or form chains (1D), layers (2D) or frameworks (3D). Although it is true for many systems that the magnetic dimensionality follows the dimensionality of the crystal structure, real situations are often more complex, especially for 0D cases. There, the magnetic dimensionality is ruled by (i) the orientation of neighbouring plaquettes and (ii) the position of anion groups formed by non-magnetic atoms that bridge the magnetic plaquettes. In most cases, the connection between structural peculiarities and the appropriate magnetic model cannot be accounted for by applying simple empirical rules (for instance, Goodenough–Kanamori–Anderson rules [32]–[34]).

Therefore, an almost complete understanding of the macroscopic magnetic behaviour for a certain system of this class can be achieved only based on a relevant microscopic model. The latter can be constructed either by using advanced experimental techniques (for instance, inelastic neutron scattering) or theoretical (DFT) calculations. Naturally, the most reliable
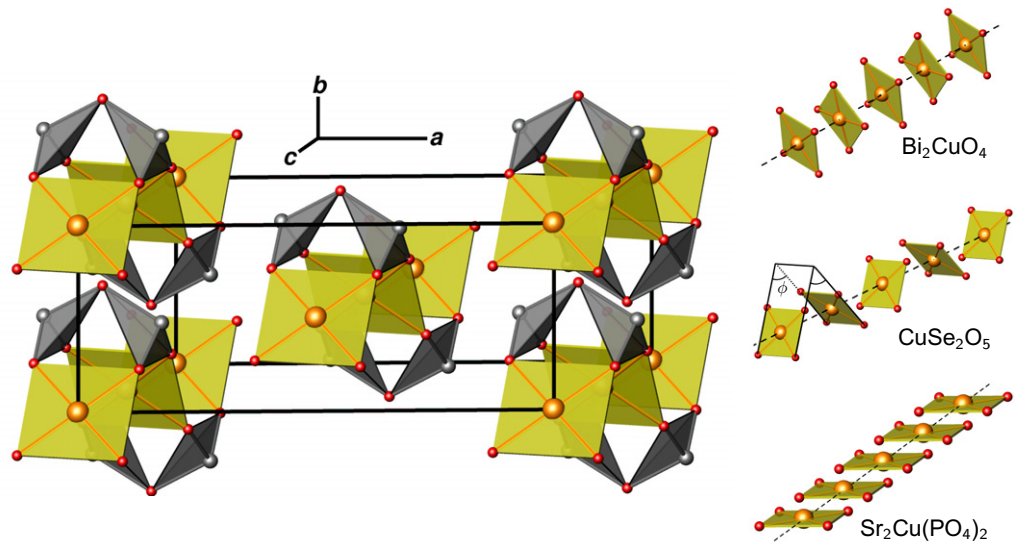
Figure 1. Left panel: the crystal structure of $CuSe_2O_5$. Isolated CuO_4 plaquettes (yellow) are bridged by SeO_3 pyramids (grey) and form chains running along c. The chains are closely stacked in b direction, and well separated in the a direction. Right panel: geometry of 'chains' formed by isolated CuO_4 plaquettes. Neighbouring plaquettes are stacked and twisted with respect to each other in Bi_2CuO_4 (top), tilted in $CuSe_2O_5$ (middle) and form planar edge-sharing chains with every second plaquette cut out in $Sr_2Cu(PO_4)_2$ (bottom). The non-magnetic groups (BiO_4, SeO_3 and PO_4 for Bi_2CuO_4, $CuSe_2O_5$ and $Sr_2Cu(PO_4)_2$, respectively) bridging the neighbouring plaquettes are not shown.

approach is the combination of such a theory and experiment. Due to the complexity of such an analysis, it has been accomplished only for a rather limited number of real systems.

Two well studied systems of this class—Bi_2CuO_4 [35] and $Sr_2Cu(PO_4)_2$ [8]—are both structurally 0D cuprates, but antipodes with respect to their magnetic behaviour. A drastic change of the magnetic coupling regime originates from the arrangement of neighbouring plaquettes (figure 1, right panel: top and bottom): stacking (accompanied by additional twisting) of neighbouring plaquettes on top of each other makes Bi_2CuO_4 a 3D magnet with $T_N \approx$ 47 K [36] while in $Sr_2Cu(PO_4)_2$ the plaquettes are arranged in a planar fashion (formally reminiscent of an edge-sharing chain with every second plaquette cut out), leading to a pronounced 1D behaviour and a very low Néel temperature $T_N = 0.085$ K [9]. In this context we mention that the magnetic dimensionality of these systems is controlled by the dihedral angle ϕ between neighbouring plaquettes (figure 1, right panel, middle). In $CuSe_2O_5$, the magnetic plaquettes are isolated (like in Bi_2CuO_4 and $Sr_2Cu(PO_4)_2$) but tilted with respect to each other forming a dihedral angle ϕ of about $64°$, i.e. in between $\phi = 0°$ for the 3D Bi_2CuO_4 and $\phi = 180°$ for the 1D $Sr_2Cu(PO_4)_2$ (figure 1, right panel). Another controlling parameter is the direct Cu–Cu distance d. Again, $CuSe_2O_5$ with d close to 4 Å lies in between $d = 2.9$ Å for Bi_2CuO_4 and $d = 5.1$ Å for $Sr_2Cu(PO_4)_2$. Thus, $CuSe_2O_5$ is structurally in between the two closely related systems: the 3D magnet Bi_2CuO_4 and the 1D magnet $SrCu_2(PO_4)_2$. Does this analogy hold also for the magnetism? To answer this question, additional arguments have to be addressed.

Besides ϕ and d, further structural features provide a deeper insight into the crystal chemical aspects relevant for the magnetism. In $CuSe_2O_5$, two SeO_3 pyramids sharing an oxygen atom (forming Se_2O_5 polyanions) bridge neighbouring CuO_4 plaquettes (see figure 1). This structural peculiarity is reflected in the morphology of the synthesized crystals (section 2): the needle-like shape with an elongation along [001] fits perfectly to structural chains along c (figure 1) formed by alternation of CuO_4 plaquettes and Se_2O_5 polyanion groups. From the topological similarity of this structural chain to the one in the structure of $Sr_2Cu(PO_4)_2$ (there, neighbouring plaquettes are bridged by two PO_4 tetrahedra) a 1D behaviour of $CuSe_2O_5$ might be expected. A second argument supports this proposition: in $CuSe_2O_5$, the structural chains are not connected by covalent bonds, making a strong IC coupling unlikely, similar to $Sr_2Cu(PO_4)_2$, where the neighbouring chains are well separated by Sr cations. These similarities of $CuSe_2O_5$ and $Sr_2Cu(PO_4)_2$ may lead to the conclusion that both systems imply essentially the same physics. However, a closer inspection of more subtle crystal chemical aspects immediately reveals an important difference related to the IC coupling. As follows from the microscopic model [8], in $Sr_2Cu(PO_4)_2$ there are two relevant NN IC couplings (2.7 K), which are equivalent by symmetry. Together with an intra-chain NN coupling (187 K), they induce magnetic frustration which commonly leads to a considerable decrease of the ordering temperature ($T_N = 0.085$ K). In $CuSe_2O_5$, these two IC couplings are not symmetry-equivalent. Therefore, by reducing the strength of one of them, the frustration can be lifted.

So far, crystal chemical considerations provided us with a qualitative insight. For a quantitative model, a microscopic analysis is required. Thus, in the next section a microscopic model based on the results of DFT calculations is constructed.

A prerequisite for an accurate modelling based on a band structure code is reliable structural information. For $CuSe_2O_5$, two refinements of the same structural model (space group $C2/c$ with four formula units per cell) have been proposed so far [37, 38]. Both structural data sets agree quite well with each other and with the lattice parameters of the synthesized samples (see table 1).[5] The reliability of the structural data has been indirectly confirmed *a posteriori* by the good agreement of calculated and experimentally measured quantities.

4. Results and discussion

4.1. Thermodynamical measurements

The first probe for the magnetic properties of a certain system is the measurement of magnetization (M) at various temperatures in a constant field (H) yielding the temperature dependence of magnetic susceptibility ($\chi(T) = M(T)/H$). This measurement already yields valuable information on the magnetic dimensionality, the sign and the energy scale of leading couplings, the presence of a spin gap, the spin anisotropy and the quality (defects, purity) of a sample.

For $CuSe_2O_5$, the magnetic susceptibility curves for both field orientations (figure 2, left panel) have a broad maximum at $T_{max} \approx 101$ K and a finite value of χ at the lowest temperature measured (1.8 K), indicating the low-dimensional behaviour and the absence of a

---

[5] It is well known, that x-ray diffraction analyses may result in considerable inaccuracies for internal coordinates of light elements (especially hydrogen). These inaccuracies can have a large impact on the magnetic properties [39]. Since there are no light atoms in $CuSe_2O_5$, we rely on the diffraction analysis and therefore, no structural relaxation has been performed.
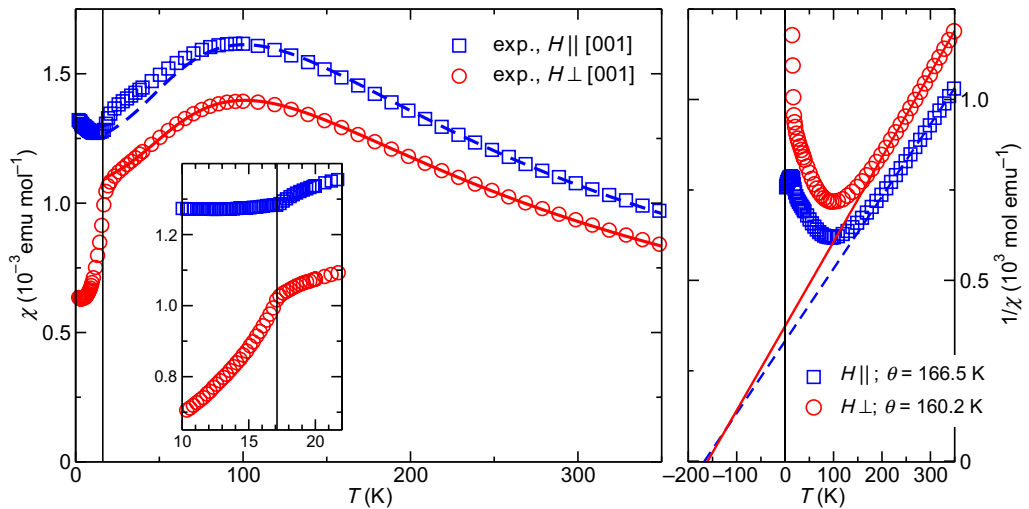
Figure 2. Left panel: magnetic susceptibility of CuSe$_2$O$_5$ as a function of temperature. The magnetizing field is 10 kOe. For the graphic presentation, we show only one of each five measured points. The Bethe ansatz fits are shown with dashed ($J = 157.1$ K, $g = 2.14$) and solid ($J = 157.6$ K, $g = 2.00$) lines. Inset: the region around the magnetic ordering temperature is shown enlarged. Right panel: inverse magnetic susceptibility as a function of temperature. Curie–Weiss fits (for $T > 230$ K) are shown with lines. The temperature-independent contribution χ_0 in the Curie–Weiss fits was set to zero.

spin gap. The high-temperature parts of the curves obey the Curie–Weiss law $\chi(T) = C/(T + \theta)$ (figure 2, right panel; $T > 220$ K, $H_\parallel$: $\theta = 165$ K, $C = 0.51$ emu mol^{-1}, $g = 2.32$; $H_\perp$: $\theta = 170$ K, $C = 0.43$ emu mol^{-1}, $g = 2.15$). The positive Curie–Weiss temperature evidences that the dominating couplings in CuSe$_2$O$_5$ are AFM. The shape of the experimental curve reveals a close similarity to a spin-1/2 Heisenberg chain model. This model has an exact solution given by Bethe ansatz [5] and parameterized by Johnston *et al* ([40] see table 1, fit 2). We have fitted the experimental curves using the parameterized solution (figure 2, left panel).

To account for the deviation of the fitted curves from experimental ones we have fitted both curves independently[6] and varied the temperature window. As a result, the magnetic susceptibility measured perpendicular to needle-like crystallites can be perfectly fitted by a consistent set of parameters ($J = 157.6$ K, $g = 2.00$) in the whole temperature range down to the ordering temperature, while the fit to the susceptibility measured parallel to the chains ($J = 157.1$ K, $g = 2.14$) shows deviations at low temperatures (below $T_{\max}$). This difference likely originates from a slight misalignment of microscopic plates in the needle-like crystallites.

A phase transition is observed at 17 K for both orientations of the magnetizing field. The nature of this magnetic transition can be understood by examination of the low-temperature part of the curve (below the transition). The interpretation is straightforward as soon as we account for (i) impurity effects and (ii) effects of misalignment of the sample (relevant especially for

---

[6] A simultaneous fit of both curves implying the same J value in the whole temperature range down to the phase transition yields considerable deviations from experiment. The origin of this deviation is discussed below in the text.

$\vec{H}_{\parallel}$, as shown above). Due to the high quality of samples, the temperature region between the kink at 17 K down to 10 K is practically unaffected by defects (no Curie tail). In this range, $\chi_{\perp}$ decreases very slightly, while $\chi_{\parallel}$ drops distinctly on cooling, following the theoretical result for ordered collinear antiferromagnets [34]. We attribute the slight decrease of $\chi_{\perp}$ (theory predicts it to be constant) to a small misalignment of crystallites, in agreement with the deviations of the Bethe ansatz fit. The small upturn in $\chi_{\parallel}$ at about 6 K (a zero susceptibility at zero temperature follows from theory) is likely related to defects and paramagnetic impurities.

To obtain an additional information about the magnetic properties, we measured the temperature dependence of the specific heat. The clear anomaly at 17 K (figure 3) and the linear behaviour of $C_p/T^2(T)$ below this temperature are typical for antiferromagnets [41]. Thus, we interpret this as a transition to an AFM ordered state ($T_N = 17$ K). Remarkably, the anomaly neither shifts nor decreases in amplitude in magnetic fields up to $\mu_0 H = 9$ T. Prior to the analysis of the magnetic behaviour above T_N, the specific heat should be decomposed into the magnetic contribution (which reflects the spectrum of magnetic excitations) and the phonon contribution (the spectrum of lattice vibrations). This decomposition is reliable only if the overlap of the two spectra (magnetic excitations and phonons) is relatively small (see [42] for an example). As the phonon contribution increases on temperature, the decomposition is possible for systems with weak magnetic couplings ($J_{ij} < 10$ K). As we obtained from our susceptibility data, the energy scale of J in $CuSe_2O_5$ is about 165 K. Thus, for a 1D Heisenberg chain we expect the maximum of the magnetic specific heat at $0.48J$ [40], i.e. close to 80 K. At this temperature, the phonon contribution to the specific heat strongly dominates over the magnetic contribution. As a result, the experimental curve has no visible features in the vicinity of 80 K. For systems with large couplings ($J_{ij} > 10$ K), the most accurate way to account for the phonon part is to measure an isostructural non-magnetic reference system (see [43] for an example). In case of $CuSe_2O_5$, it is not possible, as $ZnSe_2O_5$ has a different crystal structure [44], and thus a different phonon spectrum. Therefore, the specific heat data provide clear evidence of an AFM ordering at 17 K but do not allow an independent justification of the temperature scale for the leading magnetic interactions.

The last remark concerns a pronounced kink at 7 K (figure 3, inset), i.e. the region of the ordered phase. The kink is stable at least up to $\mu_0 H = 9$ T and thus not related to defects. Intriguingly, a similar feature has been observed for a related system Bi_2CuO_4 (figure 3 in [45]) favouring the intrinsic nature of the kink rather than a sample dependent effect. For the magnetic contribution to the specific heat, such features have been proposed to mark a dying out of high frequency spin wave modes [46]. To elucidate this unusual feature, further experimental studies on $CuSe_2O_5$ and similar systems as well as a careful theoretical analysis should be carried out.

4.2. Microscopic model

We start in our microscopic analysis with band structure calculations performed in the LDA. LDA yields a valence band of about 9 eV width formed mainly by Cu 3d, O 2p and Se 4p states (figure 4, right panel). The well-separated double-peak at the Fermi level ε_F contains two narrow, half-filled bands (figure 4, left panel). The width of this antibonding band complex (0.85 eV) is in between the widths of the same complex in Bi_2CuO_4 (1.05 eV [35]) and $Sr_2Cu(PO_4)_2$ (0.65 eV [8]). The LDA yields a metallic GS, contrary to the experimentally observed insulating behaviour. This discrepancy is caused by the underestimate of strong on-site Coulomb interactions of the Cu 3d electrons. Nevertheless, LDA reliably yields the
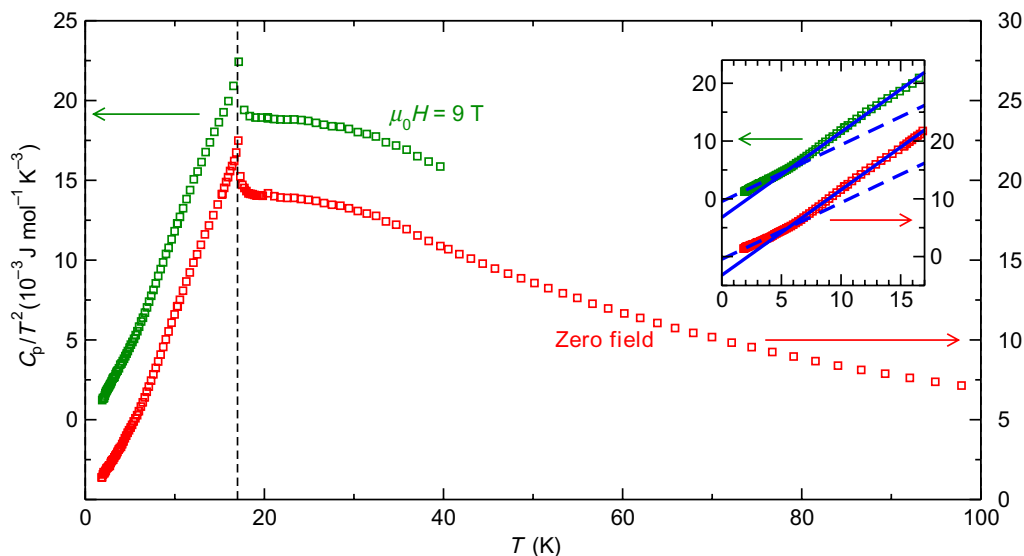
Figure 3. C_p/T^2 of $CuSe_2O_5$ as a function of temperature and magnetic field. The Néel temperature is marked with a dashed line. Inset (ordered phase region): the $C_p \sim T^3$ behaviour predicted by theory is complicated by a clear kink at 7 K.
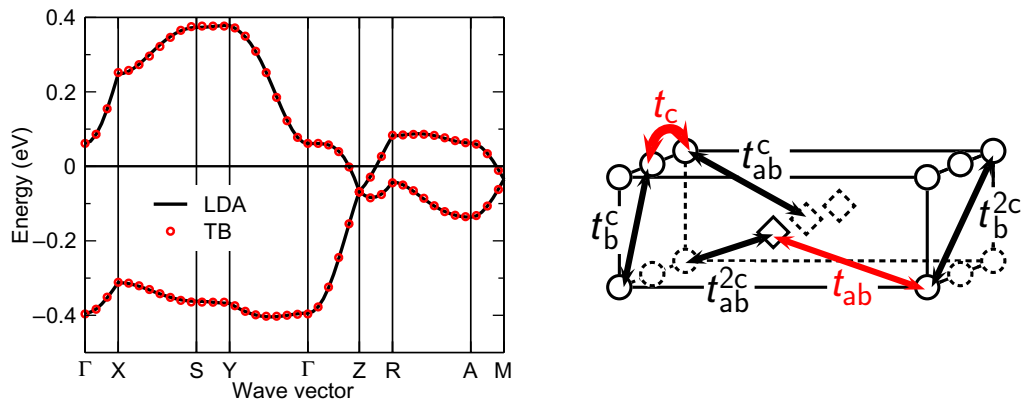
relevant orbitals and dispersions. Thus, we have a closer look to the band complex at ε_F. The two bands, relevant for the low-lying magnetic excitations, are related to the antibonding dpσ orbital of a CuO_4 plaquette, i.e. the antibonding combination of Cu $3d_{x^2-y^2}$ and O $2p_\sigma$ states (orbitals are denoted with respect to the local coordinate system). The antibonding dpσ orbital is well separated ($\Delta E \sim 0.5$ eV) from the lower lying Cu 3d and O 2p states. Thus, the most efficient way to describe the electronic structure is to construct an effective one-band TB model (one band per plaquette), parameterized by a set of electron transfer integrals t_{ij}. The correlation effects, insufficiently described by LDA and thus by the TB model, are accounted for by adopting a corresponding Hubbard model mapped subsequently onto a Heisenberg model (this mapping is valid for spin excitations in the strongly correlated limit at half-filling, both well justified for undoped cuprates with small magnetic exchange).

Prior to numerical calculations, we compare the dispersions of the two well separated bands at ε_F (figure 5) to dispersions of the corresponding antibonding dpσ complexes of $Sr_2Cu(PO_4)_2$ (figure 2 in [8]) and Bi_2CuO_4 (figure 5 in [35]). Here, a close similarity of $CuSe_2O_5$ and $Sr_2Cu(PO_4)_2$ is revealed: both band structures have a dominating dispersion along the chain direction (for $CuSe_2O_5$, this is the c-axis in figure 1 and Γ–Z region in figure 4) and a weaker dispersion in other directions, unlike Bi_2CuO_4, where the dispersions along different directions in the k-space are comparable, indicating a 3D behaviour.

For a quantitative analysis, we constructed an effective one-band TB Hamiltonian and determined the set of transfer integrals t_{ij} in order to obtain the best least-squares fit to the two LDA bands crossing ε_F. As an alternative approach, we used a Wannier functions (WF) technique which implies the construction of WF for the Cu $3d_{x^2-y^2}$ antibonding state, relevant for the magnetism, and the calculation of the overlap of the WF. The results of the latter method are affected by the overlap of the relevant $3d_{x^2-y^2}$ antibonding state with other states. Therefore, for perfectly separated bands as in $CuSe_2O_5$, both methods should yield the
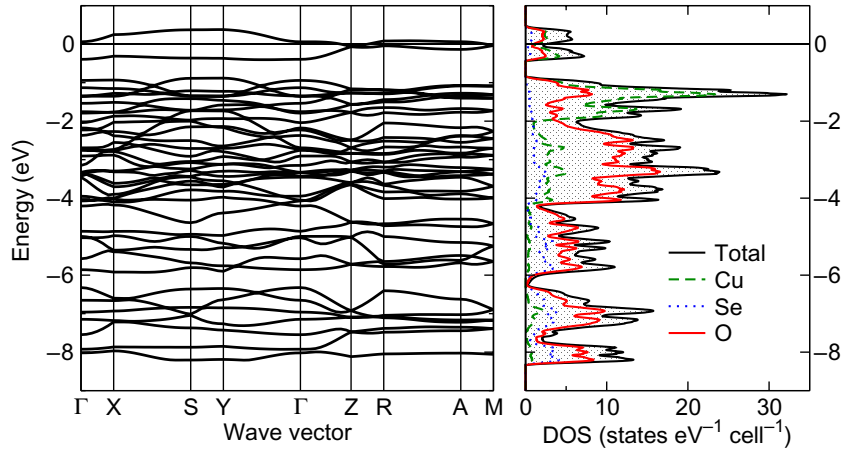
Figure 4. LDA band structure (left panel) and density of states (right panel) of $CuSe_2O_5$. Notation of k-points: $\Gamma = (000)$, $X = (\frac{\pi}{a}\,0\,0)$, $S = (\frac{\pi}{a}\,\frac{\pi}{b}\,0)$, $Y = (0\,\frac{\pi}{b}\,0)$, $Z = (0\,0\,\frac{\pi}{c})$, $R = (\frac{\pi}{a}\,0\,\frac{\pi}{c})$, $A = (\frac{\pi}{a}\,\frac{\pi}{b}\,\frac{\pi}{c})$, $M = (0\,\frac{\pi}{b}\,\frac{\pi}{c})$.

Figure 5. Left panel: the TB fit (circles) to the LDA band structure (antibonding dpσ band, solid line) Right panel: the superexchange paths for the leading transfer integrals. The projection of the structure is the same as in figure 1.

same results within numerical accuracy. The numerical evaluation supports this statement: the difference between the transfer integrals obtained by the WF method and by the TB fit is tiny and does not exceed 2 meV for individual t_{ij} values (the mean value for all t_{ij} is 0.2 meV). This deviation can be considered as an error margin for the mapping procedure. Thus, for isolated bands the WF method should not be regarded more accurate than a direct TB fit, but rather as an independent alternative procedure [10]–[12]. The agreement of the results using the two independent mapping methods reflects the applicability of an effective one-band approach.

The resulting set of the transfer integrals (table 2, first column) yields perfect agreement with the LDA bands (figure 5).[7] The hopping paths corresponding to the leading terms are shown in figure 5 (right panel).

[7] To check the results for consistency, we have neglected all t_{ij} smaller than 10 meV and repeated the fitting. The difference of leading terms in both approaches did not exceed 10%.

Table 2. Leading transfer (first column) and exchange integrals (last column) of $CuSe_2O_5$. The AFM exchange (second column) is calculated via mapping the transfer integrals onto an extended Hubbard ($U_{eff} = 4.5\,eV$) and subsequently onto a Heisenberg model. The total exchange is taken from $LSDA + U$ total energy calculations of supercells. The FM exchange J_{ij}^{FM} is evaluated as the difference between J_{ij} and J_{ij}^{AFM}.

| Path	t_{ij}(meV)	J_{ij}^{AFM}(K)	J_{ij}^{FM}(K)	J_{ij}(K)
X_c	166	285	-120	165
X_{ab}	51	27	-7	20
X_b^{2c}	11	1.5	0	1.5
X_{ab}^c	10	1	0	1
X_b^c	10	1	0	<1
X_{ab}^{2c}	7	0.5	0	<1

We find that the leading couplings in $CuSe_2O_5$ are the NN intra-chain coupling $t_c = 165\,meV$ and one of the short IC couplings $t_{ab} \approx 45\,meV$ (table 2). The corresponding WFs are pictured in figure 6. The value of the largest (NN intra-chain) coupling in $CuSe_2O_5$ is slightly larger than the corresponding coupling in $Sr_2Cu(PO_4)_2$ (135 meV [8]). The difference in the largest IC term is more pronounced: the size of the IC coupling in $CuSe_2O_5$ (45 meV, table 2) is considerably higher than in $Sr_2Cu(PO_4)_2$ (16 meV [8]). Even more important is the difference in the specific coupling geometry—whether it is constructive towards the long-range ordering or not. As we stated while comparing the crystal structures of $CuSe_2O_5$ and $Sr_2Cu(PO_4)_2$ (see section 3), in both systems there are two short IC coupling paths. The corresponding couplings are identical (symmetry-related) in $Sr_2Cu(PO_4)_2$, but independent (and in fact, considerably different) in $CuSe_2O_5$. The TB analysis reveals that only one (t_{ab}) of the two NN IC couplings is relevant for $CuSe_2O_5$ (table 2). Consequently, the essential difference between the two systems can be best understood in terms of the spin lattices that are formed by the strongest intra-chain and IC couplings, as depicted in figure 7. In $Sr_2Cu(PO_4)_2$, three relevant couplings (the intra-chain NN coupling and two identical IC couplings) are arranged on an anisotropic triangular lattice (figure 7, left panel). By switching off one of the IC couplings, the topology of the relevant couplings changes, and the system is described by two couplings forming an anisotropic square lattice (figure 7, right panel). The main difference between the two topologies is that in $Sr_2Cu(PO_4)_2$ the competition of relevant couplings, which cannot be simultaneously satisfied, leads to strong magnetic frustration, while in $CuSe_2O_5$ the IC couplings are not frustrated. The lifting of frustration in $CuSe_2O_5$ has a remarkable influence on the physical properties as will be discussed below.

The calculated transfer integrals provide valuable information on the coupling regime. To include the missing Coulomb interaction U_{eff}, as described in section 2, we can use the TB model to construct a Hubbard model and map the latter onto a Heisenberg model to obtain the AFM exchange from $J_{ij}^{AFM} = 4t_{ij}^2/U_{eff}$. Using the same representative $U_{eff} = 4.5\,eV$ as for $Sr_2Cu(PO_4)_2$ [8], we obtain $J_c^{AFM} = 285\,K$ for the NN intra-chain exchange and $J_{ab}^{AFM} = 27\,K$ for the largest IC exchange. Other couplings yield values of AFM exchange less than 1.5 K (table 2, second column) and will be neglected in further discussion.
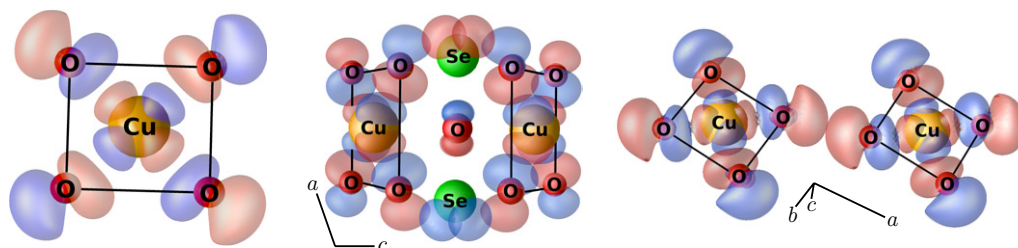
Figure 6. WF for the Cu $3d_{x^2-y^2}$ orbital. Colours represent the sign of a WF. Left panel: the Cu $3d_{x^2-y^2}$ WF plotted on top of a CuO_4 plaquette, visualizing the antibonding combination of Cu $3d_{x^2-y^2}$ and O $2p_\sigma$ states, relevant for the magnetism. Central panel: the overlap of two WF centred on the neighbouring Cu atoms (corresponds to the NN intra-chain coupling t_c). Note that the neighbouring plaquettes are tilted which leads to a sizable π-overlap of the WF, and hence O 2p wavefunctions of the neighbouring plaquettes, allowing for a considerable ferromagnetic (FM) contribution to the magnetic exchange. Right panel: the overlap of the WF corresponding to the leading IC coupling t_{ab}.
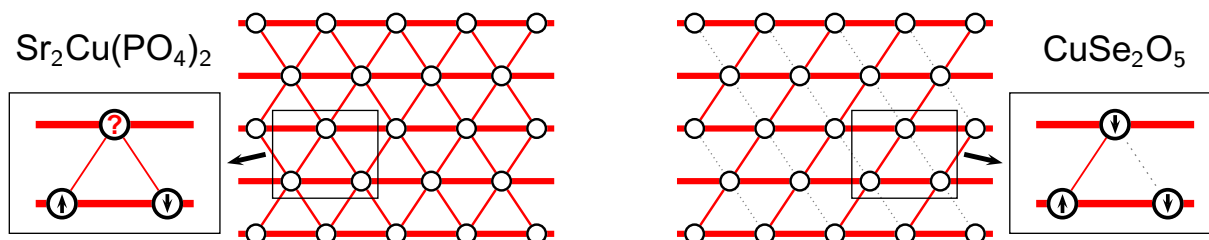
Figure 7. Topology of IC couplings in $Sr_2Cu(PO_4)_2$ (left panel) and $CuSe_2O_5$ (right panel). Red lines denote the AFM coupling. Bold red lines highlight the chains. In $Sr_2Cu(PO_4)_2$, the intra-chain and the two equivalent IC couplings form an anisotropic triangular lattice. In $CuSe_2O_5$, there is only one relevant IC coupling resulting in an anisotropic square lattice geometry of intra-chain and IC couplings. The former geometry leads to magnetic frustration, while the latter is not frustrated (see insets).

The calculated leading magnetic exchange $J_c^{AFM} = 285\,K$ is considerably larger than our estimate from the Bethe ansatz fit ($\approx 155\,K$) based on experimental $\chi(T)$ data. Moreover, it is larger than the corresponding exchange integral in $Sr_2Cu(PO_4)_2$ (187 K). This discrepancy originates from FM contributions to the total magnetic exchange, which are neglected in the mapping procedure. For the NN exchange J_c, we expect a considerable FM contribution originating from the overlap of O 2p wave functions of neighbouring plaquettes. Due to a dihedral angle $\phi = 64°$ between the neighbouring plaquettes, this overlap has a sizable π contribution (this can be seen in the WF in figure 6, central panel) leading to a Hund's rule (FM) coupling. For the leading IC coupling, the FM contribution is expected to be small due to a predominantly σ overlap of O 2p wavefunctions (figure 6, right panel).

To obtain a numerical estimate for the FM contribution, we perform total energy calculations for various spin patterns of magnetic supercells using the LSDA + U method.

The method is rather sensitive to the U_d value. As $U_d = 6.5$ eV yields agreement between the calculated and experimentally measured exchange integrals of the well studied La_2CuO_4 and $CuGeO_3$, we adopted this value in the calculations for $CuSe_2O_5$.[8] The supercell method has limitations set by numerical accuracy for the small exchange integrals ($J_{ij} < 1$ K) and the size of the required supercells. In our case, we constructed supercells and spin patterns that yield all exchange couplings which were found to be relevant from the TB analysis. The resulting total energies are mapped onto a Heisenberg model, which is parameterized by the total exchange integrals (table 2, last column) containing both AFM and FM contributions. Thus, by subtracting the AFM part J_{ij}^{AFM} from the total exchange J_{ij}, the FM contribution J_{ij}^{FM} can be estimated (table 2, fourth column).

In general, LSDA + U calculations yield a reliable estimate for exchange integrals [8, 13, 35, 42]. This reliability holds for $CuSe_2O_5$: we obtain $J_c = 165$ K and $J_{ab} = 20$ K, in almost perfect agreement with the estimates from magnetic susceptibility. In accordance with our expectations, $J_c^{FM} = -120$ K has a considerable contribution to the total exchange J_c, while $J_{ab}^{FM} = -7$ K yields a smaller correction to the J_{ab} value. We should note that the large FM contribution $J_c^{FM} = -120$ K may originate, in addition to the mentioned π-overlap of O 2p wavefunctions, from a destructive interference of coupling paths [47] or by a strong coupling to ligands [48]. Which of these mechanisms plays a leading role in $CuSe_2O_5$ is an open question. This issue is, however, beyond the scope of the present paper and needs further theoretical investigation.

Though the calculated J_c value (165 K) is very close to the estimate from the Bethe ansatz (157 K), we decided to check the exchange integrals for consistency by performing additional calculations for $U_d = 6.0$ eV and $U_d = 7.0$ eV. Besides the expected change of exchange integrals (0.5 eV increase of the U_d results in about 20% decrease of J_{ij} and vice versa), we found that the ratio $\alpha \equiv J_{ab}/J_c$ of the leading exchange integrals ($\alpha = 0.121$ for $U_d = 6.0$ eV, $\alpha = 0.129$ for $U_d = 6.5$ eV and $\alpha = 0.136$ for $U_d = 7.0$ eV) is rather stable with respect to the U_d value.

Thus, the consideration of the FM contribution yielded a valuable improvement of the energy scale comparing to the AFM exchange values J_c^{AFM} and J_{ab}^{AFM}, but the ratio α of the two couplings, that is the most relevant for the magnetic GS, stays almost unchanged. Moreover, this ratio is stable with respect to the model parameters U_{eff} and U_d, leading to a very reliable physical picture: $CuSe_2O_5$ can be described as a quasi-1D system with AFM chains characterized by an NN intra-chain exchange of 165 K. Each chain is coupled to two neighbouring chains by the non-frustrated IC exchange of 20 K (one order of magnitude smaller that the intra-chain coupling).

One of the main characteristics of the magnetically ordered state is the value of the magnetic moment. Though the corresponding theoretical values can be calculated by LDA or LSDA + U, these values are usually strongly overestimated compared to the experimentally observed magnetic moments. This discrepancy originates from strong quantum fluctuations, which are relevant especially for 1D and quasi-1D systems, and are not taken into account properly by present-day DFT approximations like LDA or LSDA + U. Therefore, to estimate the ordered magnetic moment, using the formula 19 from [6] we obtain the magnetic moment

---

[8] It is worth noting that the U_d parameter is not universal and depends on a calculational scheme and consequently on the basis set implemented in a code. Thus, different U_d values adopted in this work for $CuSe_2O_5$ ($U_d = 6.5$ eV, the code fplo version 7.00-27) and for $Sr_2Cu(PO_4)_2$ ($U_d = 8.0$ eV [8], the code fplo version 5.00-18) originate from the different basis used in the codes.
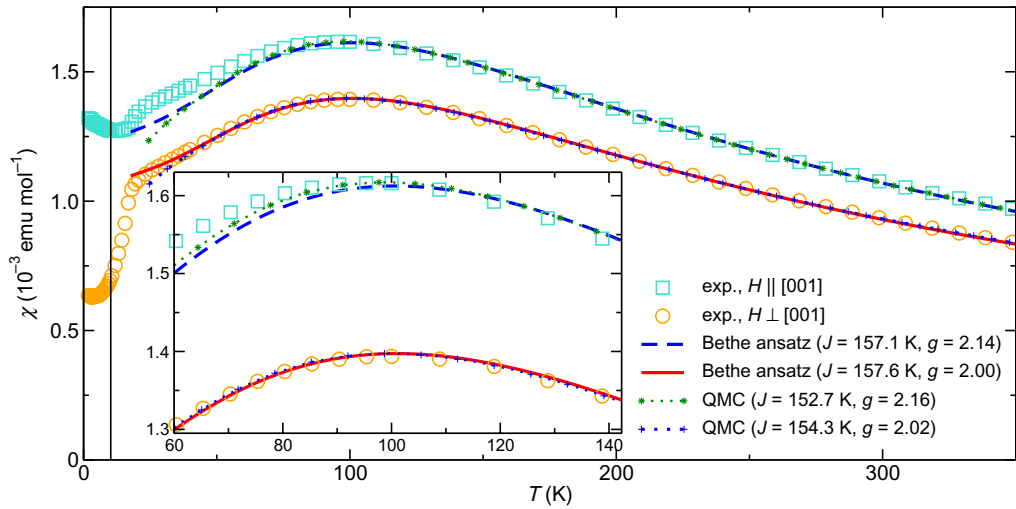
Figure 8. Comparison of Bethe ansatz and QMC fits to the experimental magnetic susceptibility. The temperature-independent contribution χ_0 in both fits was set to zero.

$m_0 = \gamma \sqrt{J_{ab}/J_c} \approx 0.25 \pm 0.05 \, \mu_B$ at zero temperature. This prediction should be challenged by future experiments.

4.3. Simulations

Turning back to the discussion about the ordering temperature (section 1), it is reasonable to point out the advantages of $CuSe_2O_5$ as a model system. Firstly, we have evidence from both theory and experiment that the system is mainly 1D. Secondly, the microscopic analysis revealed that the NNN intra-chain coupling is practically absent leading to a valuable simplification for a theoretical analysis. Finally, there is only one relevant IC coupling. The fact that this latter coupling is not frustrated allows us to use the powerful QMC method for a simulation of thermodynamical data with a subsequent comparison to the experimentally measured curves. The results of the simulations are given in figure 8 in comparison with the Bethe ansatz fits (where the IC coupling is neglected). Obviously, the inclusion of the IC coupling yields only a tiny improvement with respect to the Bethe ansatz fits. This fact demonstrates *a posteriori* the importance of a microscopic model for systems like $CuSe_2O_5$: apart from the microscopic modelling, there is no reliable way to account for the small IC coupling directly from measurements of the paramagnetic susceptibility.

4.4. Estimation of the Néel temperature

To benefit from the unique combination of the simple microscopic picture and the experimentally well-determined AFM ordering temperature T_N, we make an attempt to estimate T_N from an available simplified theory using the calculated exchange integrals. Still, there are three problems, intrinsic for quasi-1D systems, to be accounted for. The first is the spatial anisotropy of exchange couplings present in a system. This problem is resolved in $CuSe_2O_5$ only partially. On one hand, there is only one relevant IC coupling for every pair of neighbouring

Table 3. Exchange integrals (columns 2 and 3) together with experimental (column 5) and theoretically calculated (columns 7–10) ordering temperatures T_N for quasi-1D cuprates (3D magnet Bi_2CuO_4 has a similar structural motive and was added for completeness). The ordering temperatures T_N were calculated using formulae from references [20, 22, 24] and the exchange integrals from columns 2 (NN intra-chain coupling J_1) and 3 (leading IC coupling $J_\perp$). Note that the first four systems are frustrated due to IC couplings, while in the last two the IC couplings are not frustrated.

Compound	J_1(K)	$J_\perp$(K)	Ref.	T_N exp. (K)	Ref.	T_N calc. (K)			
						[20]	[22]	[24]	[35]
Sr_2CuO_3	2200	9	[6]	5	[49]	28	22	21	
Ca_2CuO_3	1850	42	[6]	9	[49]	115	91	85	
$Sr_2Cu(PO_4)_2$	187	3	[8]	0.085	[50]	8.5	6.7	6.3	
$K_2CuP_2O_7$	196	0.25	[13]	< 2	[13]	0.9	0.7	0.6	
$CuSe_2O_5$	165	20		17		23	18	17	
Bi_2CuO_4	10	6	[35]	42	[36]				47

chains, but on the other hand, it couples a certain chain with only two of four neighbouring chains. Thus, the couplings to the other two chains are considerably smaller, resulting in the (spatial) exchange anisotropy. The second problem is the anisotropy in the spin space. In our microscopic approach, we used the isotropic Heisenberg model where this anisotropy is neglected. Although we observe a remarkable agreement between the microscopic model and the macroscopic behaviour, the spin anisotropy is present, as evidenced for instance by the strong dependence of the *g*-factor on the orientation of a magnetizing field (figure 2). In a common sense approach, the (spatial) exchange anisotropy is expected to lower T_N, while the spin anisotropy raises it. In each system, these two effects are balanced. Attempts to find a suitable description for this balance were made in a number of advanced theoretical studies based on a mean-field formalism [19, 20], [22]–[25]. Still, the problem seems not to be resolved, since a considerable disagreement remains between the numerical results yielded by different theories (none of which is generally accepted) and, even more important, due to the third problem—the problem of IC magnetic frustration, which has not been addressed so far.

Here, we make an empirical attempt to estimate how the frustration influences the magnetic ordering. For that purpose, we compare several quasi-1D magnetic compounds in a systematic way. The two well studied quasi-1D cuprates Sr_2CuO_3 and Ca_2CuO_3 are commonly referred to as model systems in most theoretical studies regarding the T_N problem. We should note that these two systems are essentially different from $CuSe_2O_5$ due to the presence of corner-sharing chains of CuO_4 plaquettes, which results in one order of magnitude larger NN coupling. In addition, the NNN coupling is not negligible [6]. Nevertheless, they are referred here for the sake of completeness. In both, Sr_2CuO_3 and Ca_2CuO_3, one of the relevant IC couplings is frustrated. To calculate T_N, we use formulae given by Schulz [20], Irkhin and Katanin [22] and Yasuda *et al* [24]. The calculated T_N are given in the three last columns of (table 3). Disregarding the method used, the calculated T_N considerably overestimate the experimental values for Sr_2CuO_3 and Ca_2CuO_3 (table 3, fifth column).

A theoretical approach is expected to work better for systems with more pronounced 1D nature—e.g. $Sr_2Cu(PO_4)_2$ and $K_2CuP_2O_7$. The structural peculiarities of these systems were

discussed in section 3. The main issue here is the frustration caused by the leading IC coupling. For $Sr_2Cu(PO_4)_2$, theory predicts an ordering temperature T_N two orders of magnitude larger than the experimentally observed value. (Unfortunately, experimental low-temperature data are not available for $K_2CuP_2O_7$.) This huge discrepancy is in sharp contrast with the situation for the 3D magnet Bi_2CuO_4, for which the theoretical estimate coincides with the experimental value (table 3, last row).[9]

In $CuSe_2O_5$, each chain is strongly coupled only with two of four neighbouring chains (unlike Sr_2CuO_3, Ca_2CuO_3, $Sr_2Cu(PO_4)_2$ and $K_2CuP_2O_7$ with coupling to four neighbouring chains). There is no unique way to take this feature into account. A simple approximation is to take the arithmetic average, which yields an effective IC coupling value $J_\perp = J_{ab}/2$.[10] Using this value, theory yields a perfect agreement with experimental value (table 3, fifth row).

Obviously, the existing models describe the magnetic ordering in $CuSe_2O_5$ much better than in Sr_2CuO_3 and Ca_2CuO_3, and especially in $Sr_2Cu(PO_4)_2$. Despite our crude way of accounting for spatial exchange anisotropy and the neglect of spin anisotropy, the theoretical estimate of T_N for $CuSe_2O_5$ is in surprisingly good agreement with the experimental value. Though in general the magnetic ordering is affected by the spin anisotropy, $CuSe_2O_5$ yields empirical evidence that for systems with a small spin anisotropy the isotropic model provides a rather accurate estimate of T_N. Thus, it is unlikely that the disagreement between theoretical and experimentally observed T_N values for $Sr_2Cu(PO_4)_2$ originates from the neglect of spin anisotropy effects.

Finally, only the magnetic frustration is left to be a possible reason for a huge discrepancy between theory and experiment. Our analysis reveals that frustrated IC couplings play a crucial role for the magnetic ordering. This fact explains why theoretical schemes fail to predict T_N for frustrated systems.

To illustrate the influence of frustration, we use a simple formula from the spin wave theory in a random phase approximation, which connects Néel temperatures for two compounds A and B with the values of exchange integrals: $T_N^A/T_N^B \approx \sqrt{J_1^A J_\perp^A}/\sqrt{J_1^B J_\perp^B}$ [6]. Using the values of exchange integrals for $Sr_2Cu(PO_4)_2$ and $CuSe_2O_5$ and the experimental Néel temperature for $Sr_2Cu(PO_4)_2$ (table 3), we obtain $T_N \approx 0.146$ K for $CuSe_2O_5$, almost 120 times smaller than the experimental value.

In the existing theoretical approaches, a parameter controlling the frustration caused by IC couplings is missing. Therefore, new theories which would treat magnetic frustration as one of the key issues for the magnetic ordering, are needed. On the other hand, there is a lack of information from the experimental side, resulting in a very limited number of systems that challenge the theoretical predictions. Besides $CuSe_2O_5$, an almost perfect model system, synthesis and investigation of new systems with similar crystal chemistry are highly desirable.

5. Summary and outlook

The class of quasi-1D magnets attracts much attention as a field of search for prominent models and a playground for modern theories. Recently, by studying the magnetic properties of Cu^{2+}

---

[9] For the theoretical estimation of T_N, the formula (7) from [35] was used.

[10] Alternatively, the geometrical averaging can be used. This approach yields a correct limit with respect to the Mermin–Wagner theorem (zero ordering temperature for 1D and 2D systems). Then, calculational schemes from [20], [22] and [24] yield T_N values of 14, 11 and 10 K, respectively.

phosphates, several systems of this class were found to exhibit the physics of a Heisenberg chain model. In these materials, the remarkable one-dimensionality and the absence of long-range intra-chain interactions are ruled by a unique arrangement of magnetically active CuO_4 plaquettes: they form edge-sharing chains where every second plaquette is cut out. The chains are well separated by alkaline or alkaline earth cations (K, Sr). The magnetic susceptibility of these systems is perfectly described by the Bethe ansatz, which provides an exact solution for the NN AFM spin-1/2 Heisenberg chain. At the same time, the ordering temperature T_N of the systems reveals a fundamental disagreement between theory and experiment. Unfortunately, the range of available experimental studies of these systems is rather limited, as the materials are currently available only as powders.

Therefore, we have synthesized $CuSe_2O_5$—a system implying a similar, isolated arrangement of neighbouring CuO_4 plaquettes (but tilted with respect to each other, unlike Cu^{2+} phosphates) and allowing for a growth of high quality single crystals. Thermodynamic measurements reveal a quasi-1D behaviour with a leading AFM coupling of about $160\,K$ (obtained from the Bethe ansatz fit for the magnetic susceptibility). The system orders antiferromagnetically at $17\,K$, as evidenced by magnetic susceptibility and specific heat data. A microscopic analysis based on the results of DFT calculations reveals that $CuSe_2O_5$ can be described in good approximation by only two relevant exchange integrals: NN intra-chain ($J_c = 165\,K$) and the leading IC coupling ($J_{ab} = 20\,K$). The theoretical estimate of the ordering temperature T_N is in perfect agreement with experimental value. This remarkable agreement is in sharp contrast with a huge overestimate of T_N for Cu^{2+} phosphates yielded by a formal application of the same theory. To reveal the origin of this difference on empirical grounds we analysed systematically the factors affecting T_N. Beyond the influence of the spatial exchange anisotropy and the spin anisotropy, we emphasize the role of the magnetic frustration due to equivalent IC interactions in the latter compounds. Comparing theoretical and experimental data for related systems, we show that IC frustrations have a crucial influence on T_N and are likely the main cause for the failure of any theory which ignores them.

For an outlook, we propose further experimental studies (for instance, Raman spectroscopy and inelastic neutron scattering) in order to benefit from the availability of single crystals of $CuSe_2O_5$. In particular, additional experimental data are required in order to understand the nature of the specific heat anomaly at $7\,K$. Secondly, we hope that our work will inspire a directed search for new quasi-1D model systems. Last, but not least, we want to stimulate the development of more sophisticated theories for the estimation of T_N. In particular, such theories should explicitly take into account the magnetic frustration arising from complex IC interactions. The well understood system $CuSe_2O_5$ could give valuable support for these theories.

IOP Institute of Physics · DEUTSCHE PHYSIKALISCHE GESELLSCHAFT

References

[1] Hase M, Terasaki I and Uchinokura K 1993 *Phys. Rev. Lett.* **70** 3651–4
[2] Enderle M *et al* 2005 *Europhys. Lett.* **70** 237–43
[3] Drechsler S-L *et al* 2007 *Phys. Rev. Lett.* **98** 077202
[4] Schmitt M, Málek J, Drechsler S-L and Rosner H 2009 *Phys. Rev.* B **80** 205111
[5] Bethe H 1931 *Z. Phys.* **71** 205–26
[6] Rosner H, Eschrig H, Hayn R, Drechsler S-L and Málek J 1997 *Phys. Rev.* B **56** 3402
[7] Ami T, Crawford M K, Harlow R L, Wang Z R, Johnston D C, Huang Q and Erwin R W 1995 *Phys. Rev.* B **51** 5994–6001
[8] Johannes M D, Richter J, Drechsler S-L and Rosner H 2006 *Phys. Rev.* B **74** 174435
[9] Belik A A, Azuma M and Takano M 2004 *J. Solid State Chem.* **177** 883–8
[10] Salunke S S, Ahsan M A H, Nath R, Mahajan A V and Dasgupta I 2007 *Phys. Rev.* B **76** 085104
[11] Rosner H, Schmitt M, Kasinathan D, Ormeci A, Richter J, Drechsler S-L and Johannes M D 2009 *Phys. Rev.* B **79** 127101
[12] Salunke S, Ahsan M A H, Nath R, Mahajan A V and Dasgupta I 2009 *Phys. Rev.* B **79** 127102
[13] Nath R, Kasinathan D, Rosner H, Baenitz M and Geibel C 2008 *Phys. Rev.* B **77** 134451
[14] Farnell D J J and Parkinson J B 1994 *J. Phys: Condens. Matter* **6** 5521–32
[15] Okamoto K and Nomura K 1992 *Phys. Lett.* A **169** 433–7
[16] Chitra R, Pati S, Krishnamurthy H R, Sen D and Ramasesha S 1995 *Phys. Rev.* B **52** 6581–7
[17] Tonegawa T and Harada I 1989 *J. Phys. Soc. Japan* **58** 2902–15
[18] Mermin N D and Wagner H 1966 *Phys. Rev. Lett.* **17** 1133–6
[19] Scalapino D J, Imry Y and Pincus P 1975 *Phys. Rev.* B **11** 2042–8
[20] Schulz H J 1996 *Phys. Rev. Lett.* **77** 2790–3
[21] Essler F H L, Tsvelik A M and Delfino G 1997 *Phys. Rev.* B **56** 11001–13
[22] Irkhin V Y and Katanin A A 2000 *Phys. Rev.* B **61** 6757–64
[23] Bocquet M 2002 *Phys. Rev.* B **65** 184415
[24] Yasuda C, Todo S, Hukushima K, Alet F, Keller M, Troyer M and Takayama H 2005 *Phys. Rev. Lett.* **94** 217201
[25] Todo S and Shibasaki A 2008 *Phys. Rev.* B **78** 224411
[26] Zvyagin A A and Drechsler S-L 2008 *Phys. Rev.* B **78** 014429
[27] Kahn O, Verdaguer M, Girerd J J, Galy J and Maury F 1980 *Solid State Commun.* **34** 971–5
[28] Koepernik K and Eschrig H 1999 *Phys. Rev.* B **59** 1743–57
[29] Perdew J P and Wang Y 1992 *Phys. Rev.* B **45** 13244–9
[30] Eschrig H, Koepernik K and Chaplygin I 2003 *J. Solid State Chem.* **176** 482–95
[31] Albuquerque A F *et al* 2007 *J. Magn. Magn. Mater.* **310** 1187–93
[32] Goodenough J B 1955 *Phys. Rev.* **100** 564–73
[33] Kanamori J 1959 *J. Phys. Chem. Solids* **10** 87–98
[34] Goodenough J B 1963 *Magnetism and the Chemical Bond* (New York: Interscience-Wiley)
[35] Janson O, Kuzian R O, Drechsler S-L and Rosner H 2007 *Phys. Rev.* B **76** 115119
[36] Petrakovskii G A, Sablina K A, Pankrats A I, Vorotinov V M, Furrer A, Roessli B and Fischer P 1995 *J. Magn. Magn. Mater.* **140–144** 1991–2
[37] Meunier G, Svensson C and Carpy A 1976 *Acta Crystallogr.* B **32** 2664
[38] Becker R and Berger H 2006 *Acta Crystallogr.* E **62** I256–7
[39] Janson O, Richter J and Rosner H 2008 *Phys. Rev. Lett.* **101** 106403
[40] Johnston D C, Kremer R K, Troyer M, Wang X, Klümper A, Bud'ko S L, Panchula A F and Canfield P C 2000 *Phys. Rev.* B **61** 9558–606
[41] Stølen S, Grande T and Allan N L 2004 *Chemical Thermodynamics of Materials* (Chichester: Wiley)
[42] Nath R, Tsirlin A A, Rosner H and Geibel C 2008 *Phys. Rev.* B **78** 064422

IOP Institute of Physics ⦶ DEUTSCHE PHYSIKALISCHE GESELLSCHAFT

[43] Kondo S *et al* 1997 *Phys. Rev. Lett.* **78** 3729–32
[44] Meunier G and Bertaud M 1974 *Acta Crystallogr.* B **30** 2840–3
[45] Baran M, Gaidukov Y P, Danilova N P, Inushkin A V, Jedrzejczak A, Koksharov Y A, Nikiforov V N, Revcolevschi A, Szymczak R and Szymczak H 1999 *J. Magn. Magn. Mater.* **196–197** 532–3
[46] Tari A 2003 *The specific heat of matter at low temperatures* (London: Imperial College Press) p 148
[47] Feldkemper S, Weber W, Schulenburg J and Richter J 1995 *Phys. Rev.* B **52** 313–23
[48] Geertsma W and Khomskii D 1996 *Phys. Rev.* B **54** 3011–4
[49] Kojima K M *et al* 1997 *Phys. Rev. Lett.* **78** 1787–90
[50] Belik A A, Uji S, Terashima T and Takayama-Muromachi E 2005 *J. Solid State Chem.* **178** 3461–3